

UC San Diego

UC San Diego Previously Published Works

Title

Evaluation of normal cadaveric Achilles tendon and enthesis with ultrashort echo time (UTE) magnetic resonance imaging and indentation testing

Permalink

<https://escholarship.org/uc/item/9h27k0p1>

Journal

NMR in Biomedicine, 32(1)

ISSN

0952-3480

Authors

Chen, Bimin
Cheng, Xin
Dorthe, Erik W
[et al.](#)

Publication Date

2019



DOI

10.1002/nbm.4034

Peer reviewed

RESEARCH ARTICLE

Evaluation of normal cadaveric Achilles tendon and enthesis with ultrashort echo time (UTE) magnetic resonance imaging and indentation testing

Bimin Chen^{1,2} | Xin Cheng^{3,2} | Erik W. Dorth⁴ | Yinghua Zhao² | Darryl D'Lima⁴ |
Graeme M. Bydder² | Sirun Liu¹ | Jiang Du²  | Ya-Jun Ma² 

¹Department of Radiology, The First Affiliated Hospital of Jinan University, Guangzhou, China

²Department of Radiology, University of California, San Diego, CA, USA

³Department of Histology and Embryology, Medical School, Jinan University, Guangzhou, China

⁴Shiley Center for Orthopedic Research and Education at Scripps Clinic, La Jolla, CA, USA

Correspondence

Ya-Jun Ma, Ph.D., University of California, San Diego, Department of Radiology, San Diego, CA 92103-8226, USA.

Email: yam013@ucsd.edu

Funding information

NIH, Grant/Award Numbers: 1R01 AR068987-01 and R01 AR062581-01A1; Medical Scientific Research Foundation of Guangdong Province, Grant/Award Number: A201789

Entheses are regions where tendons and ligaments attach to bone, and are the primary target in seronegative and other diseases of the musculoskeletal (MSK) system. MRI has been widely used for visualizing features of inflammatory and degenerative MSK disease; however, normal tendons and entheses have short transverse relaxation times (T_2), and show little or no signal with conventional clinical MRI pulse sequences, making it difficult to investigate their MR properties. In this study we examined the normal MR morphology of the cadaveric Achilles tendon and enthesis at 3 T using novel three-dimensional ultrashort echo time (3D UTE) Cones sequences, and at 11.7 T using conventional MRI sequences. We also studied the MR properties of the Achilles tendon and enthesis including T_2^* , T_1 , and magnetization transfer ratio (MTR). In addition, MT modeling of macromolecular proton fractions was investigated using 3D UTE Cones sequences at 3 T. Indentation testing was performed to investigate the mechanical properties of the tendons and entheses, and this was followed by histological examination. In total five specimens (<50 years) were investigated. On average, tendons and entheses respectively had T_2^* values of 0.93 ± 0.48 ms and 2.77 ± 0.79 ms, T_1 values of 644 ± 22 ms and 780 ± 55 ms, MTRs of 0.373 ± 0.03 and 0.244 ± 0.009 with an MT power of 1000° and frequency offset of 2 kHz, and macromolecular proton fractions of $18.0 \pm 2.2\%$ and $13.9 \pm 1.9\%$. Compared with the tendon, the enthesis generally had a longer T_2^* , a longer T_1 , a lower MTR, and a lower macromolecular proton fraction as well as both a higher Young's modulus and stiffness. Results from this study are likely to provide a useful baseline for identifying deviations from the normal in seronegative arthritis and other disease of the entheses.

KEYWORDS

Achilles tendon, enthesis, indentation testing, ultrashort echo time

Abbreviations used: 3D UTE, three-dimensional ultrashort echo time; FA, flip angle; FOV, field of view; FSE, fast spin echo; GRE, gradient recalled echo; MSK, musculoskeletal; MT, magnetization transfer; MTR, magnetization transfer ratio; SpA, spondyloarthritis
Bimin Chen and Xin Cheng made equal contributions.

1 | INTRODUCTION

In the human body, tendons and ligaments perform the function of transferring force from muscle to bone in order to execute movements. At the junction between tendons or ligaments and bone, the mechanical load is distributed by entheses.¹ These consist of uncalcified fibrocartilage and calcified fibrocartilage and are situated between the fibrous connective tissue of tendon and cortical bone. The fibrocartilage resists compressive loads and shear forces and disperses mechanical stress, which is concentrated at the hard-soft tissue interface spanned by the enthesis. Failure to disperse the stress may lead to acute and overuse injuries in sports such as tennis or golfer's elbows and jumper's knee.¹⁻³

The importance of entheses extends beyond traumatic and overuse injuries. Disease at these sites is often described as enthesopathy and can occur in many disorders, including traumatic, degenerative, inflammatory, endocrine and metabolic conditions.^{2,3} In some cases, enthesopathy represents the initial and predominant manifestation in conditions such as the seronegative spondyloarthropathies (SpAs).⁴ Enthesitis is common in SpA patients and occurs in synovial joints, the Achilles tendon enthesis, the plantar fascia and other sites.⁴⁻⁶

MRI has been widely used for visualizing the features of arthritis and traumatic disease,⁶ but conventional clinical MRI has not been helpful for demonstrating and characterizing the key normal tissues present in tendons and entheses. These tissues typically have short apparent transverse relaxation times (T_2)^{1,7} and show little or no signal with conventional clinical pulse sequences.^{8,9}

We have developed three-dimensional ultrashort echo time (3D UTE) pulse sequences with nominal T_E values much shorter than those of clinical sequences.¹⁰⁻¹² These UTE sequences allow us to directly image the clinically "MR invisible" Achilles tendon and its enthesis. In this study, we aimed to investigate the MR morphology of Achilles tendons and entheses at 3 T and 11.7 T, then assess their MR properties, including T_2^* , T_1 , magnetization transfer ratio (MTR) and magnetization transfer (MT) modeling of parameters characterizing the water and macromolecular proton fractions of tissue using UTE sequences at 3 T. Finally, we wished to perform indentation testing to investigate the mechanical properties of the Achilles tendon and enthesis, and correlate the results from this with the MR findings.

2 | METHODS AND MATERIALS

2.1 | Specimen preparation

In total five ankle specimens from young donors (three females, two males, average age 35.4 ± 5.0 years, age range 28–40 years) were obtained from the University of California, San Diego (UCSD) Medical School Anatomical Preparation Laboratory. All the ankle specimens used in this study were from donors without a history of diseases such as inflammatory arthropathy or trauma involving the ankle. The specimens were stored fresh frozen in a -80°C freezer ((Bio-Freezer; Forma Scientific, Marietta, OH, USA). Each specimen was thawed overnight to room temperature and imaged at 3 T. After this each specimen was sectioned into thin slices (~ 3 mm thickness) for high resolution imaging on a Bruker 11.7 T system (Bruker BioSpec, Ettlingen, Germany). The specimens were sectioned again for indentation testing and finally for histology.

2.2 | MRI

MR data were acquired using a 3D UTE Cones sequence implemented on a 3 T MR750 scanner (GE Healthcare Technologies, Milwaukee, WI, USA) with a maximum gradient performance of 50 mT/m and 200 mT/m/ms. A knee coil was used for data acquisition. Morphological imaging was performed with the basic 3D UTE Cones sequence, which employed a short rectangular pulse (duration 52 μs) for signal excitation followed by spiral sampling with conical view ordering.¹¹ Conventional clinical gradient echo and fast spin echo (FSE) sequences, including T_1 and proton density weighted imaging, were performed for comparison. Quantitative imaging at 3 T was performed with a dual-echo 3D UTE Cones sequence to measure T_2^* (two sets of dual echoes with T_E values of 0.032/4.4 ms and 0.4/8.8 ms, $T_R = 20$ ms, a flip angle or FA of 10° , fat saturated). 3D UTE Cones variable FA (VFA) acquisitions were used to measure T_1 ($T_R = 20$ ms, FA = 5° , 10° , 20° , and 30° , $T_E = 0.032$ ms) with B_1 correction using actual FA mapping ($T_R = 20/100$ ms, FA = 45° , $T_E = 0.032$ ms).¹³ A Cones MT sequence was used to measure MTR with a series of MT frequency offsets ($\Delta f = 2, 5, 10, 20$, and 50 kHz) and MT powers ($\theta = 400^\circ, 600^\circ, 800^\circ, 1000^\circ$). To accelerate the UTE-Cones MT data acquisition, multiple spokes ($n = 11$) were utilized with each MT preparation pulse.¹⁴ Other imaging parameters included a bandwidth (BW) of 166 kHz, a field of view (FOV) of 11 cm, a slice thickness of 2 mm, 36 slices, acquisition matrix of 256×256 , total scan time of 8 min for T_2^* measurement, 31 min for T_1 measurement, and 43.3 min for MTR and MT modeling, respectively.

Morphological imaging was performed on a 11.7 T system (Bruker BioSpec) with a maximum gradient performance of 750 mT/m and 6600 T/m/s. A birdcage coil was used for signal excitation and data acquisition. The higher field strength and much more powerful gradient and RF systems were expected to result in a much improved signal to noise ratio, allowing higher spatial resolution imaging of fine structure in the Achilles tendon and enthesis. A conventional 2D gradient recalled echo (GRE) sequence was performed with the following imaging parameters: bandwidth of 110 kHz, FOV of 4×3 cm, FA = 50° , $T_R = 800$ ms, $T_E = 3.2$ ms, slice thickness 1 mm, 10 slices, acquisition matrix 400×226 , total scan time 3 min.

A quantitative MRI data analysis algorithm was written in MATLAB (MathWorks, Natick, MA, USA) and was executed offline on the DICOM images obtained using the protocols described above. T_2^* was obtained via single-component exponential fitting of the two dual-echo 3D UTE

Cones images. T_1 was obtained via single-component fitting of the 3D UTE Cones images acquired with different FAs.¹³ MTR was calculated as the ratio of signal difference without and with the MT pulse applied over the signal without the MT pulse. MT modeling was performed using a modified rectangular pulse approximation model (RP model) on data acquired with a multi-spoke 3D UTE-Cones MT sequence. Details of the algorithm have been reported elsewhere.¹⁴

2.3 | Indentation testing

Indentation testing was performed on each enthesis slice. We used a previously reported rapid indentation test for measuring local compressive stiffness.¹⁵ Tissue specimens were hydrated with phosphate-buffered saline containing proteinase inhibitors. A matrix of test sites was mapped onto the surface of the Achilles tendons and entheses. Each of the test sites was subjected to indentation testing to obtain force-displacement data. Using a custom bench top apparatus (two-axis grippers, SMAC, Carlsbad, CA, USA; 50 g load cell, FUTEK, Irvine, CA, USA) fitted with a 0.48 mm diameter stainless steel plane-ended tip, three locations were tested within a 1 mm area. The loading protocol consisted of application of a 0.02 N tare load, followed by a ramp compression to 125 μm at 50 $\mu\text{m}/\text{s}$, a pause at the peak depth for 1 s, and a release. Measurement at each point was repeated three times and the force results were averaged. A field of points was selected to encompass the area of interest in each specimen covering the enthesis and nearby Achilles tendon. The peak force at each location was measured, recorded, and averaged. The average peak force was used to calculate structural indentation stiffness (the peak force divided by the indentation depth). We also computed the elastic modulus, using a linear elastic model assuming a Poisson's ratio of 0.5.¹⁶

2.4 | Histology

Standard histologic procedures were applied to the tissue blocks, which were sectioned at 8 μm slice thickness in the sagittal plane with 12 slices collected at 1 mm intervals throughout the block. Alternate sections were stained with Masson's trichrome and toluidine blue. MR images were overlaid on histological indentation maps by visually aligning the outer edges of the specimen.

3 | RESULTS

Figure 1 shows representative histology of the normal Achilles tendon and enthesis. The Achilles tendon and enthesis show distinct structural differences. The Achilles tendon appears as a dense fibrous connective tissue (Figure 1A-C), while the enthesis shows uncalcified and calcified fibrocartilage including a basophilic line at the tidemark. This represents a region at which calcification has ceased and calcium has subsequently accumulated (Figure 1D-F).

Figure 2 shows selected 3D UTE Cones images of a cadaveric Achilles tendon and enthesis specimen, clinical T1w and PDw images at 3 T, and a high resolution GRE image obtained at 11.7 T. The clinical sequences show near zero signal for the Achilles tendon and intermediate signal for

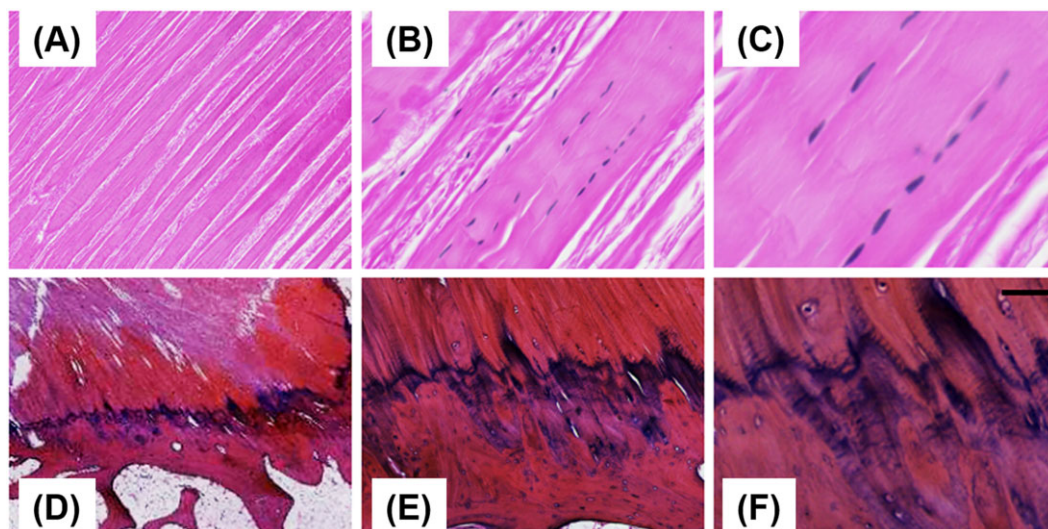


FIGURE 1 Histological images of an ankle specimen, demonstrating normal Achilles tendon (A-C) and enthesis (D-F) using hematoxylin and eosin (HE) staining. Scale bar, 1 mm in A and D, 200 μm in B and E, 50 μm in C and F. The fibrous connective tissue tendon is seen at progressively higher resolution from A to C. Tendon, uncalcified fibrocartilage, basophilic tidemark, calcified fibrocartilage, and cortical bone are seen in D-F at progressively higher resolution

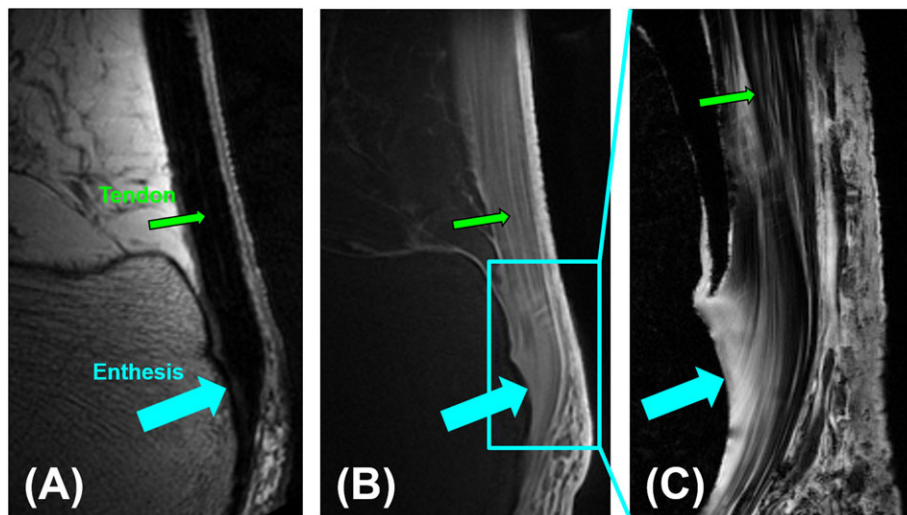


FIGURE 2 Morphological imaging of a cadaveric human ankle specimen at 3 T using clinical T1w FSE sequence (A) and 3D UTE Cones sequence with fat suppression (B), as well as at 11.7 T imaging using a GRE sequence (C). The upper green arrows in A-C show the Achilles tendon. The lower broad blue arrows in images A-C show the enthesis. This is poorly seen in A, appears uniformly intermediate in B and has a relatively high signal in C

part of the enthesis (arrow), while the 3D UTE Cones sequence shows intermediate signal for both tendon and enthesis (arrow). The 11.7 T image shows greater detail including high contrast between the tendon and enthesis (arrow).

Figure 3 shows representative single-component T_2^* fitting for the Achilles tendon and enthesis, respectively. A short T_2^* of 0.74 ± 0.11 ms was demonstrated for the Achilles tendon, while a longer T_2^* of 2.69 ± 0.48 ms was demonstrated for the enthesis. Enteses have longer T_2^* values, which is consistent with the higher signal observed at 11.7 T, using a relatively long T_E of 3.2 ms.

Figure 4 shows UTE MT images acquired with four frequency offsets (2, 5, 10, and 20 kHz) with an MT power of 1000° . The corresponding MTR maps are also displayed. Higher MTR values were observed when lower MT frequency offsets were used. The ankle enthesis had a lower MTR than the Achilles tendon for each set of MT frequency offset and MT power values.

Figure 5 shows selected quantitative T_1 and MT fitting curves of one specimen. Excellent T_1 and two-pool MT modeling were achieved for both the Achilles tendon and enthesis. The enthesis had a longer T_1 and lower macromolecular proton fraction than the Achilles tendon.

Figure 6 illustrates the biomechanics of sampling of a representative enthesis slice. Indentation stiffness varied significantly with site, but demonstrated a significantly higher elastic modulus and stiffness for the enthesis compared with the tendon ($p < 0.001$).

Table 1 summarizes the quantitative UTE MTR measurements of the ankle specimens. The mean and standard deviation of MTR for each frequency offset and MT pulse power are displayed. For a typical MT pulse power of 1000° , the MTR for the Achilles tendon decreased from 0.373 ± 0.030 to 0.095 ± 0.010 when the frequency offset was increased from 2 kHz to 20 kHz. In comparison, the MTR for the enthesis decreased from 0.244 ± 0.009 to 0.068 ± 0.002 when the frequency offset was increased from 2 kHz to 20 kHz. A similar trend was observed at MT pulse powers of 600° and 800° . The MTR for the enthesis was about 20–40% lower than that of the Achilles tendon for each specific MT pulse power and frequency offset.

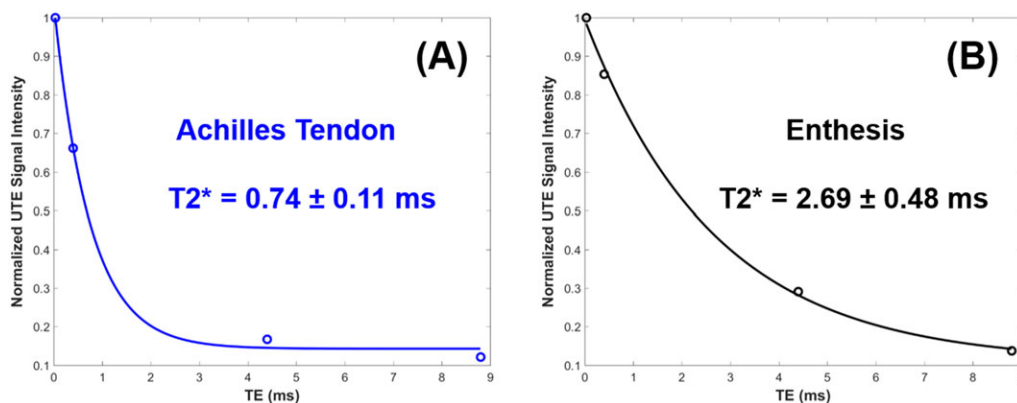


FIGURE 3 Single-component T_2^* fitting of fat saturated 3D UTE Cones images of a representative cadaveric ankle specimen. This shows a short T_2^* of 0.74 ± 0.11 ms for the Achilles tendon (A) and 2.69 ± 0.48 ms for the ankle enthesis (B). The location of the samples was as indicated by the green and blue arrows in Figure 2

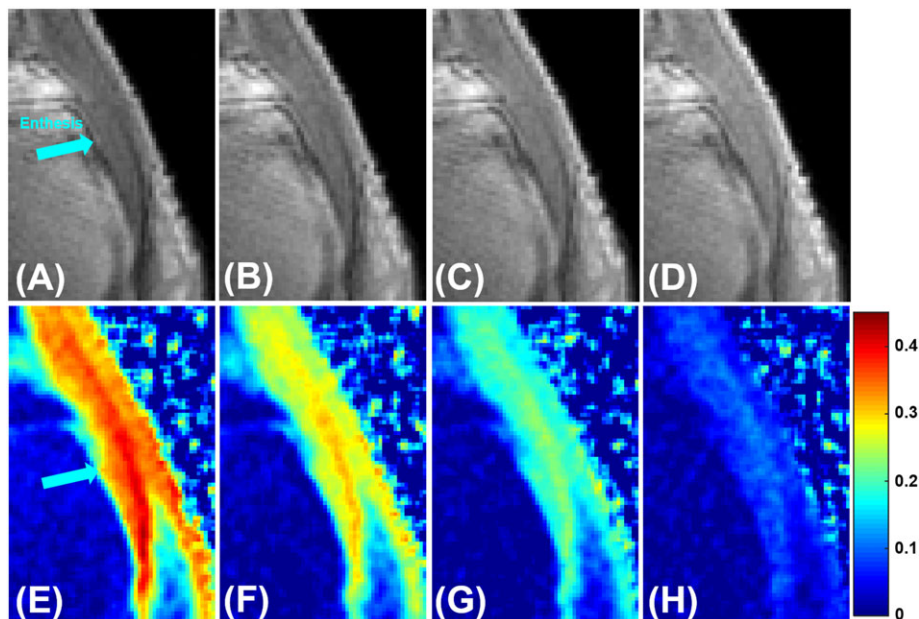


FIGURE 4 Selected 3D UTE Cones MT images of an ankle specimen acquired with different MT frequency offsets and MT powers (A-D) and the corresponding MTR maps with an MT power of 1000° and frequency offset of 2 kHz (E), 5 kHz (F), 10 kHz (G), and 20 kHz (H). The ankle entheses has a lower MTR than the Achilles tendon for each set of MT frequency offset and MT power. The blue arrows show the regions of the entheses

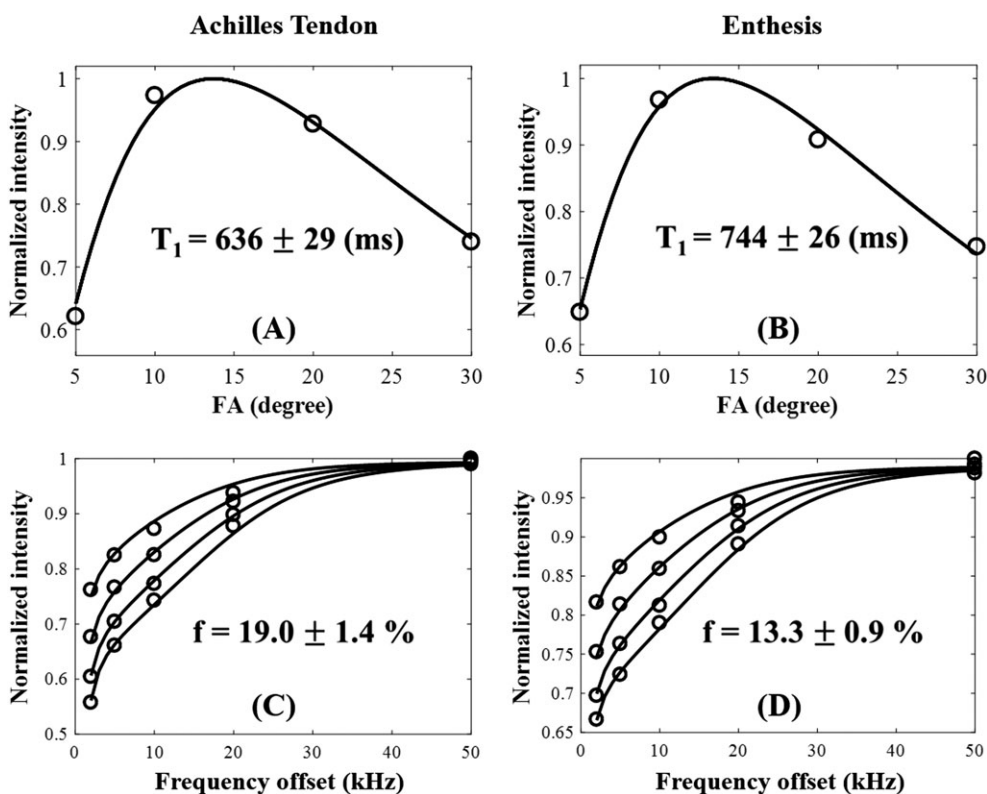


FIGURE 5 3D UTE Cones quantitative T_1 (A, B) and MT modeling (C, D) fitting curves of a representative cadaveric human ankle joint specimen. This shows a T_1 of 636 ± 29 ms for the Achilles tendon (A) and 744 ± 26 ms for the entheses (B), and a macromolecular proton fraction of $19.0 \pm 1.4\%$ (C) for the Achilles tendon and $13.3 \pm 0.9\%$ (D) for the entheses

Table 2 summarizes other quantitative UTE MRI measurements and biomechanical results for the Achilles tendon and entheses. The mean and standard deviation of each measurement, including T_2^* , T_1 , and macromolecular fraction as well as indentation testing results, are listed. Generally, compared with the Achilles tendon, the ankle entheses had a longer T_2^* , a longer T_1 , and a lower macromolecular proton fraction, as well as a higher Young's modulus and stiffness.

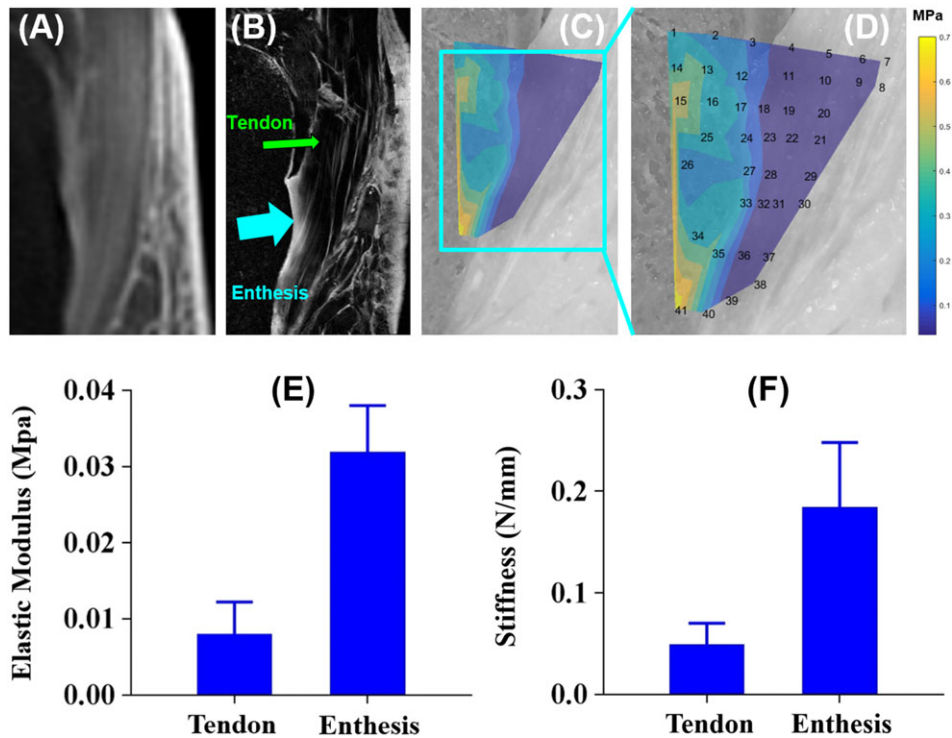


FIGURE 6 Biomechanical testing of an ankle specimen. A, B, MR images of the selected specimen slice at 3 T (A) and 11.7 T (B). C, D, Photograph and elastic modulus mapping of a small region covering both the Achilles tendon and enthesis (C), as well as an enlarged map showing selected indentation points (D). E, F, Both the Young's modulus (E) and stiffness (F) were about four times higher for the enthesis than for the Achilles tendon

TABLE 1 The mean and standard deviation of MTR measurements for the Achilles tendon and enthesis in five normal ankle specimens. The MTR data were acquired with three MT power settings of 1000°, 800°, and 600°, and four frequency offsets of 2, 5, 10, and 20 kHz

MTR		2 kHz	5 kHz	10 kHz	20 kHz
1000°	Tendon	0.373 ± 0.030	0.279 ± 0.021	0.212 ± 0.017	0.095 ± 0.010
	Enthesis	0.244 ± 0.009	0.191 ± 0.008	0.141 ± 0.002	0.068 ± 0.002
800°	Tendon	0.292 ± 0.022	0.206 ± 0.025	0.146 ± 0.013	0.071 ± 0.006
	Enthesis	0.223 ± 0.013	0.160 ± 0.020	0.107 ± 0.015	0.051 ± 0.005
600°	Tendon	0.215 ± 0.011	0.153 ± 0.007	0.115 ± 0.006	0.045 ± 0.005
	Enthesis	0.165 ± 0.006	0.120 ± 0.007	0.087 ± 0.005	0.035 ± 0.009

TABLE 2 The mean and standard deviation of T_2^* , T_1 , and MTR modeling of macromolecular proton fraction (f), as well as elastic modulus and stiffness, of the Achilles tendon and enthesis of five normal ankle specimens

	T_2^* (ms)	T_1 (ms)	f (%)	Elastic modulus (MPa)	Stiffness (N/mm)
Tendon	0.93 ± 0.48	644 ± 22	18.0 ± 2.2	0.0079 ± 0.0043	0.0486 ± 0.0216
Enthesis	2.77 ± 0.79	780 ± 55	13.9 ± 1.9	0.0319 ± 0.0061	0.1838 ± 0.0643

4 | DISCUSSION

The use of 3D UTE pulse sequences allows normal tendinous and enthesis structures that have not previously been visualized with clinical sequences to be demonstrated.

This study is the first to report high resolution morphological imaging of the Achilles tendon and enthesis at 3 T and 11.7 T. The ultrahigh field imaging at 11.7 T provides an excellent depiction of the fine details of the collagen fiber structure as well as high contrast between the Achilles tendon and enthesis. The enthesis shows distinctly higher signal, especially when imaged with a longer T_E and at higher field strength. Furthermore, the 11.7 T images with much improved enthesis contrast helps guide ROI placement, and thus more accurate quantitative evaluation of T_1 , T_2^* , MTR, and MT modeling of macromolecular proton fraction for the Achilles tendon and enthesis. It is also the first study to quantitatively evaluate the MR and biomechanical properties of the two different tissues. The ankle enthesis has significantly longer T_2^* , longer T_1 , lower MTR,

and lower macromolecular proton fractions.¹⁷⁻²⁰ In disease the T_2^* values of both tendon and enthesis are likely to be elevated, so images with longer echo times should be included for more accurate T_2^* measurement. The enthesis has higher Young's modulus and stiffness compared with the tendon. These different MR and mechanical properties can be correlated with the structural and functional differences between the two tissues. The elastic modulus and stiffness still have variations across both tendons and entheses. We think this probably reflects genuine differences in tissue collagen and in the case of entheses of calcium as well.

The Achilles tendon and enthesis are structurally different.²¹⁻²³ Enthsis contains higher concentrations of glycosaminoglycans than tensile tendon, and this is associated with increased swelling pressure and resistance to compression.²⁴⁻²⁶ The tensional regions of tendons or ligaments typically have numerous fascicles of longitudinally aligned collagen fibers separated by looser connective tissue, which merges with the epitenon or epiligament. Within the tendon/ligament matrix, sparse, elongated fibroblasts are visible. As the enthesis is approached, the structure of the tendon/ligament changes over a short distance, from the typical appearance of dense fibrous connective tissue to that of uncalcified fibrocartilage.¹ Here cells are more rounded and usually arranged in rows, although at some enthesis, there is no regular pattern discernible in the arrangement of cells. The cells are surrounded by a small amount of aggrecan-containing extracellular matrix and separated by collagen fibers, which immunolabel strongly for type II collagen. The aggrecan in the matrix gives the fibrocartilage its elevated water content and is critical to the role of fibrocartilage in resisting compression. The transition to the third zone (calcified fibrocartilage) is usually marked by a basophilic line, the tidemark (Figure 1). This represents a region at which calcification has ceased and calcium has subsequently accumulated. Under physiological conditions the tidemark is relatively straight. The fibers of tendons and ligaments continue across it (generally at right angles) as they pass from uncalcified to calcified fibrocartilage. The tidemark may be duplicated or even multiplied in cases with additional calcification fronts. The junction between calcified fibrocartilage and subchondral bone (i.e. the cement line) is highly irregular. It is the anatomic boundary between tendon or ligament and bone, and thus the true site of union of the tissues.²¹

There are several limitations of this study. First, abnormal tendons and entheses were not investigated in this study. It is a natural next step to apply the morphological and quantitative UTE MRI techniques to ankle specimens with different degrees of degeneration, and determine the value of UTE derived MRI biomarkers for predicting mechanical and histological degradation. The preliminary studies performed in this paper provide a technical basis for such further studies. Second, we did not investigate the effects of the freeze-thaw cycle on tendon and enthesis MR characteristics or tissue biomechanical properties. However, our prior studies suggest that repetitive freeze-thawing cycles have no statistically significant effect on UTE T_2^* measurement.²⁷ Third, simple single-component T_2^* was investigated rather than more complicated bi-component T_2^* analysis. Bi-component T_2^* analysis provides information on bound and free water T_2^* values and relative fractions, which may further improve the quantitative evaluation of tendons and entheses.²⁸ A single-component T_2^* analysis was performed due to its simplicity, ease of clinical application and relatively short scan time, especially as T_1 measurement together with MTR and MT modeling took over an hour with our current protocol. Further optimization is needed to reduce the total scan time.

In conclusion, we have demonstrated that high resolution morphological imaging of the Achilles tendon and enthesis can be achieved at 3 T and especially 11.7 T. The 3D UTE Cones sequences also provide quantitative measures of T_2^* , T_1 , MTR, and MT modeling of macromolecular proton fractions. These UTE measures can potentially be used as biomarkers of biomechanical degradation of the tendons and entheses, and this is likely to help in the clinical investigation of SpA and other diseases of entheses.

ACKNOWLEDGEMENT

The authors acknowledge grant support from NIH (1R01 AR062581-01A1 and 1R01 AR068987-01).

ORCID

Jiang Du  <http://orcid.org/0000-0002-9203-2450>

Ya-Jun Ma  <http://orcid.org/0000-0003-0830-9232>

REFERENCES

1. Benjamin M, Toumi H, Ralphs JR, Bydder G, Best TM, Milz S. Where tendons and ligaments meet bone: attachment sites ('enthesis') in relation to exercise and/or mechanical load. *J Anat.* 2006;208:471-490.
2. Claudepierre P, Voisin MC. The enthesis: histology, pathology, and pathophysiology. *Joint Bone Spine.* 2005;72:32-37.
3. McGonagle D, Benjamin M, Marzo-Ortega H, Emery P. Advances in the understanding of enthesal inflammation. *Curr Rheumatol Rep.* 2002;4:500-506.
4. Gossec L, McGonagle D, Korotaeva T, et al. Minimal disease activity as a treatment target in psoriatic arthritis: a review of the literature. *J Rheumatol.* 2018;45:6-13.
5. Coates LC, Conaghan PG, D'Agostino MA, et al. Remission in psoriatic arthritis—where are we now? *Rheumatology.* 2018;57:1321-1331.
6. Aydin SZ, Tan AL, Hodsgon R, et al. Comparison of ultrasonography and magnetic resonance imaging for the assessment of clinically defined knee enthesitis in spondyloarthritis. *Clin Exp Rheumatol.* 2013;31:933-936.
7. Baker JF, Conaghan PG, Emery P, Baker DG, Ostergaard M. Relationship of patient-reported outcomes with MRI measures in rheumatoid arthritis. *Ann Rheum Dis.* 2017;76:486-490.
8. Benjamin M, Bydder GM. Magnetic resonance imaging of enthesis using ultrashort TE (UTE) pulse sequences. *J Magn Reson Imaging.* 2007;25:381-389.

9. Du J, Pak BC, Znamirovski R, et al. Magic angle effect in magnetic resonance imaging of the Achilles tendon and enthesis. *Magn Reson Imaging*. 2009;27:557-564.
10. Du J, Bydder M, Takahashi AM, Carl M, Chung CB, Bydder GM. Short T2 contrast with three-dimensional ultrashort echo time imaging. *Magn Reson Imaging*. 2011;29:470-482.
11. Carl M, Bydder GM, Du J. UTE imaging with simultaneous water and fat signal suppression using a time-efficient multi-spoke inversion recovery pulse sequence. *Magn Reson Med*. 2016;76:577-582.
12. Ma YJ, Carl M, Shao H, Tadros AS, Chang EY, Du J. Three-dimensional ultrashort echo time Cones $T_{1\rho}$ (3D UTE-Cones- $T_{1\rho}$) imaging. *NMR Biomed*. 2017;30:e3709.
13. Ma YJ, Lu X, Carl M, et al. Accurate T1 mapping of short T2 tissues using a three-dimensional ultrashort echo time Cones actual flip angle-variable TR (3D UTE-Cones AFI-VTR) method. *Magn Reson Med*. 2018;80:598-608.
14. Ma YJ, Chang EY, Carl M, Du J. Quantitative magnetization transfer ultrashort echo time imaging using a time-efficient 3D multispoke Cones sequence. *Magn Reson Med*. 2017;79:692-700.
15. Villegas DF, Maes JA, Magee SD, Donahue TL. Failure properties and strain distribution analysis of meniscal attachments. *J Biomech*. 2007;40(12):2655-2662.
16. Hayes WC, Keer LM, Herrmann G, Mockros LF. A mathematical analysis for indentation tests of articular cartilage. *J Biomech*. 1970;5:541-551.
17. Juras V, Zbyn S, Pressl C, et al. Regional variations of T_2^* in healthy and pathologic Achilles tendon in vivo at 7 Tesla: preliminary results. *Magn Reson Med*. 2012;68:1607-1613.
18. Wright P, Juras V, McGonagle D, Robson M, Ridgeway J, Hodgson R. Comparison of two ultrashort echo time sequences for the quantification of T_1 within phantom and human Achilles tendon at 3 T. *Magn Reson Med*. 2012;68:1279-1284.
19. Chen B, Zhao Y, Cheng X, et al. Three-dimensional ultrashort echo time Cones (3D UTE-Cones) magnetic resonance imaging of enthesis and tendons. *Magn Reson Imaging*. 2018;49:4-9.
20. Filho GH, Du J, Pak BC, et al. Quantitative characterization of the Achilles tendon in cadaveric specimens: T1 and T2* measurements using ultrashort-TE MRI at 3 T. *Am J Roentgenol*. 2009;192(3):117-124.
21. Milz S, Rufai A, Buettner A, Putz R, Ralphs JR, Benjamin M. Three-dimensional reconstructions of the Achilles tendon insertion in man. *J Anat*. 2002;200:145-152.
22. Benjamin M, Ralphs JR. Tendons and ligaments—an overview. *Histol Histopathol*. 1997;12:1135-1144.
23. Francois RJ, Braun J, Khan MA. Enthesis and enthesitis: a histopathologic review and relevance to spondyloarthritis. *Curr Opin Rheumatol*. 2001;13:255-264.
24. Koob TJ, Vogel KG. Site-related variations in glycosaminoglycan content and swelling properties of bovine flexor tendon. *J Orthop Res*. 1987;5:414-424.
25. Okuda Y, Gorski JP, An KN, Amadio PC. Biochemical, histological, and biomechanical analyses of canine tendon. *J Orthop Res*. 1987;5:60-68.
26. Maroudas A, Bannan C. Measurement of swelling pressure in cartilage and comparison with the osmotic pressure of constituent proteoglycans. *Biorheology*. 1981;18:619-632.
27. Chang EY, Bae WC, Statum S, Du J, Chung CB. Effects of repetitive freeze-thawing cycles on T2 and T2* of the Achilles tendon. *Eur J Radiol*. 2014;83:349-353.
28. Juras V, Apprigh S, Szomolanyi P, Bieri O, Deligianni X, Trattnig S. Bi-exponential T2* analysis of healthy and diseased Achilles tendons: an in vivo preliminary magnetic resonance study and correlation with clinical score. *Eur Radiol*. 2013;23:2814-2822.

How to cite this article: Chen B, Cheng X, Dorthe EW, et al. Evaluation of normal cadaveric Achilles tendon and enthesis with ultrashort echo time (UTE) magnetic resonance imaging and indentation testing. *NMR in Biomedicine*. 2019;32:e4034. <https://doi.org/10.1002/nbm.4034>